Original Manuscript

JOURNAL OF COMPOSITE MATERIALS

Journal of Composite Materials
2025, Vol. 0(0) 1–20

DOI: 10.1177/00219983251362941
journals.sagepub.com/home/jcm
Sage

Investigation of the effect of high-entropy alloy particles on the mechanical behavior of aluminum matrix composites produced by accumulative roll bonding

Mahdi Hamounpeyma[1], Mohsen Haddad Sabzevar[1] and Mohammad Hasan Farshidi[1]

Abstract

The objective of this research is to achieve a suitable combination of strength and ductility in an aluminum matrix composite reinforced with high entropy alloy (HEA) particles by using the accumulative roll bonding (ARB) process. The novelty of this study is that several new high-entropy alloys have been used to fabricate new aluminum matrix composites by the ARB process and to find the optimal mechanical properties of the composite. For this purpose, three types of high entropy alloy with different chemical compositions were added to aluminum matrix composite by using the ARB process. The selection of high entropy alloys was based on the fact that all three types of crystal structures FCC, BCC, and FCC + BCC were formed in the composite production. The effect of the parameters of the number of rolling passes, weight percentage of HEA, and type of HEA was investigated on the tensile strength, elongation, hardness and microstructure of the composite. The results showed that the highest tensile strength and elongation were obtained for the sample produced with 2 wt% $Al_{0.4}CoCr_{0.5}NiFeTi_{0.6}$ at six rolling passes. Moreover, the highest hardness was obtained for sample produced with 4 wt% $Al_{1.5}MnCoCrNiFe$. However, the samples produced with MnCoCrNiFe indicated the lowest tensile strength.

Keywords

Accumulative roll bonding, aluminum matrix composite, high entropy alloy, tensile strength, elongation

Introduction

Today, various manufacturing technologies such as welding, soldering, machining, forming, etc. are used to produce new products with desirable microstructure and improved mechanical properties.[1–9] Aluminum alloys are widely used in the production of numerous products. This material is suitable for use in many applications, including the automotive, aerospace, and electronics industries.[10,11] Aluminum alloys can exhibit relatively high strength and ductility at a relatively low cost compared to other metals. Therefore, increasing strength or reducing modification costs could make aluminum more attractive for a wider range of applications. The mechanical, chemical, or physical properties of metal sheets can be controlled by changing its microstructure.[11–22]

Fabrication of nanoscale structures is an emerging and innovative approach to modify the structure of metals.[23] This improves the properties of materials for the industrial applications. One approach is to apply very high levels of strain to metal sheets in the form of multilayer sandwich structures, which increases the strength-to-weight ratio of the material.[23–29] Nanoscale aluminum-based sheets are attractive due to their structural integrity, ease of fabrication, exceptional strength, and low cost.[30–32] This leads to the fabrication of lighter and cheaper products with optimized life cycles. The production of nanomaterials through layered composite structures can lead to new combinations of properties of metals and alloys.[33] The main challenge in the development of this type of materials is to find a commercially feasible manufacturing method that is able to produce a suitable structure at a competitive cost.[34,35] Recently, the accumulative roll bonding (ARB) process has been developed as a promising method for producing

[1]Faculty of Engineering, Department of Materials and Metallurgical Engineering, Ferdowsi University of Mashhad, Mashhad, Iran

Corresponding author:
Mohsen Haddad Sabzevar, Faculty of Engineering, Department of Materials and Metallurgical Engineering, Ferdowsi University of Mashhad, Azadi square, Mashhad, Razavi Khorasan 9177948497, Iran.
Email: haddadm@um.ac.ir

Data Availability Statement included at the end of the article

nanostructures in the form of layered composite sheets.[33–35] In this method, two different metal sheets of the same thickness are stacked on top of each other and a 50% reduction in thickness is achieved using a single-pass rolling. In the next step of the ARB cycle, the joined sheets are cut in half and prepared for subsequent ARB cycles.[36] Accumulative roll bonding (ARB) is an effective technique for increasing the tensile strength of metal sheets through grain structure modification. In this method, successive rolling and reduction of sheet thickness results in the formation of an ultrafine grain structure (UFG). In the ARB technique, tensile strength increases with increasing work hardening and grain boundary.[37] Gholami et al.[38,39] reported that the tensile strength of composites produced by the ARB process improved after different cycles. However, products fabricated by this method exhibit low ductility because premature necking reduces the total energy required for failure.[40] Recently, to overcome this problem, composite sheets have been produced using two different materials, soft and hard.[41] The ARB process can also be used to join dissimilar materials. Heydari Vini et al.[42,43] investigated the bonding properties of Al/Cu joint obtained by ARB process. Jasim et al.[44] also used the ARB process to produce Al/Al_2O_3 bulk composites. Sajjadi Nikoo et al.[45] fabricated dissimilar laminated composite of the AA2024 and AA5083 aluminum alloys by four cycles of the ARB process. They observed that the grain size of microstructure was significantly decreased and dislocation density was increased, leading to an improvement in the tensile strength and hardness.

Adding reinforcement particles in the early cycles of ARB can create a metal composite and reinforcing particles. Reinforcing particles increase the hardness and strength of the produced composite.[46,47] Composites reinforced with hard ceramic particles such as nitrides, borides, carbides and oxides increase the strength significantly but severely reduce the ductility and machinability. On the other hand, due to the poor interface between the matrix and the ceramic particles, the force transfer to the particles is not good. Also, these particles are the site of micro-crack initiation, which reduces the fracture toughness.[48] It has been reported that the addition of nanoparticles to aluminum and magnesium matrixes has improved ductility and strength. However, one of the most important problems in the addition of nanoparticles is agglomeration and non-uniform distribution of particles.[49–54]

In recent years, high-entropy alloys (HEAs) have been used in film and bulk forms to reinforce metal matrix composites due to their excellent coating properties, corrosion resistance, high strength and ductility, and high thermal stability.[49,50,55–59] High-entropy alloys are a new class of engineering materials consisting of five or more primary elements in equimolar or non-equimolar ratios.[51,52] The atomic ratio of each element is usually between 5 and 35%. It should be noted that other nanoparticles, such as carbon nanotubes and ceramic nanoparticles, do not improve all mechanical properties simultaneously. However, HEA particles are composed of different alloying elements, each of which improves one of the mechanical properties. On the other hand, the manufacturability and cost of HEA particles are lower than other nanoparticles. Another reason for choosing high-entropy particles as reinforcements for metal matrix composites is that these particles are more compatible with the matrix from a metallurgical point of view. Also, the reduction in the flexibility of the final sample by high-entropy particles is much less than that of ceramic particles. Previous studies indicated that the use of high-entropy reinforcing particles has improved the strength, fracture toughness, and ductility of aluminum, titanium, and copper.[60,61] Tan et al.[53] improved the strength and ductility by adding high-entropy particles of $Al_{0.6}CoCrFeNi$ to aluminum matrix composite using the spark plasma sintering (SPS) method. Lu et al.[54] reported that the plasticity of the SiC-2024Al composite improved by addition of $CoNiFeCrAl_{0.6}Ti_{0.4}$ high-entropy alloy particles. Zhang et al.[62] stated that the yield strength, tensile strength and compressive strength of 2124 aluminum alloy were enhanced by adding AlCoCrFeNi high entropy alloy using spark plasma sintering. Yuan et al.[63] also used spark plasma sintering to prepare 2024 aluminum composite by addition of CoCrFeMnNi high-entropy alloy particles. They reported that the hardness of the composite increased by 63.7%. Zhu et al.[64] used FeCoNiCrAl high-entropy alloy particles to fabricate Cu matrix composites by friction stirring process and observed that the hardness, tensile strength and elongation of the fabricated composite increased by 54.86%, 17.17% and 8.4%, respectively. Xiang et al.[65] optimized the yield strength, ultimate compressive strength and compressive strain of titanium matrix composite by addition of the TiZrNbTa high-entropy alloy. LUO et al.[66] enhanced the mechanical properties of aluminum matrix composites reinforced with $Al_{0.5}CoCrFeNi$ high-entropy alloy particles using asymmetric cryorolling. They reported that the asymmetric cryorolling indicated finer grain sizes, fewer microvoids, and higher dislocation density in the aluminum matrix composite reinforced with high-entropy alloy compared to asymmetric rolling. Wang et al.[67] applied vacuum hot press sintering process to produce Ti/Al laminated composites reinforced with $Al_{0.5}CoCrFeNi$ high entropy alloy particles and reported that the materials prepared at a temperature of 730°C indicated better flexural strength and fracture toughness. Improvement of mechanical properties of metal matrix composites by adding high entropy alloys has also been reported by Zhang et al.,[68] Liu et al.,[69] Emamifar et al.,[70] Zhang et al.,[71] Konovalov et al.,[72] and Luo et al.[73] The results of previous research have also shown that the thermal stability of composites reinforced with HEA particles is good and their mechanical properties do not change much up to high temperatures.[74–77] Shadangi et al.[74] found that AA 6082 Al matrix composite reinforced with

Table 1. Different HEAs used in this research.

Type	1	2	3
Name	$Al_{0.4}Ti_{0.6}CoCr_{0.5}NiFe$	$Al_{1.5}MnCoCrNiFe$	MnCoCrNiFe
Lattice	FCC + BCC	BCC	FCC
Melting point (°C)	1755.5	1550	1735
Mesh size	250–300	270–325	260–310

AlSiCrMnFeNiCu high-entropy alloy are thermally stable up to 650°C. Sathiyamoorthi et al.[75] reported that the composite reinforced with CoCrFeNi high entropy alloy exposed to 700°C for 600 h showed negligible change in hardness and grain size. Jadhav et al.[76] reported that the room temperature FCC + BCC phases of $FeCoCrNi_2Al$ high entropy alloy remains stable up to 1000°C. Zhang et al.[77] stated that FeCoNiCu HEA particles are highly stable at high temperatures and impose a pinning effect on the grain boundaries, which significantly restricts grain growth up to 900°C. The long-term performance (fatigue and creep) of the composites reinforced with high entropy particles was also investigated by some authors. Rozman et al.[78] stated that about half of the CoCrFeNiMn creep specimens exceeded 34% strain. Liu et al.[79] observed that multi-phase high entropy alloys, particularly the metastable ones, are favorable to fatigue resistance over single-phase alloys. Song et al.[80] investigated the tensile creep behavior and mechanism of CoCrFeMnNi high entropy alloy and found that apparent dynamic recovery and recrystallization occur for creep at 973 K while high dislocation density can be observed for creep at 923 K and lower temperatures.

A review of previous research shows that composites reinforced with high entropy particles have not been produced by the ARB method. Therefore, in this research, the ARB method is used to fabricate aluminum matrix composite with high entropy reinforcing particles. In fact, the main novelty of this paper is that the ARB process is used to fabricate new aluminum matrix composites by addition of new high-entropy alloys. The selected high-entropy alloys generate BCC, FCC, and FCC + BCC crystal structures in the composite. It should be noted that the high-entropy alloy with FCC structure has good ductility, and the high-entropy alloy with BCC structure has high strength. Therefore, the high-entropy alloy with FCC and BCC structure has a good combination of ductility and strength. On the other hand, the aluminum element, which is similar to the composite matrix, is different in the three samples. The other novelty of this study is to achieve a unique combination of high tensile strength and ductility through the ARB process. Then, the microstructure of the fabricated composite was analyzed by SEM, EDS and XRD to find a relationship between the microstructure and mechanical properties. Since the strength and ductility of the produced composite are simultaneously improved, it can be used in the automotive and aerospace industries.

Materials and methods

Materials

In this research, three types of high-entropy alloy (HEA) particles with different crystal structures were used, as shown in Table 1. The chemical and physical properties of high-entropy alloys are given in Tables 2–4. HEA compositions were prepared based on the previous research[49–54] and the results of XRD analysis. It should be noted that the Al is a BCC stabilizer in HEAs. Therefore, in the first HEA compound where the Al content is low ($Al_{0.4}Ti_{0.6}CoCr_{0.5}NiFe$), the FCC + BCC structure is formed. In the second HEA compound where the Al content is increased ($Al_{1.5}MnCoCrNiFe$), the BCC structure is formed. And in the third HEA compound where the Al is removed (MnCoCrNiFe), the FCC structure is formed. It should be also stated that the Mn is a FCC stabilizer in HEAs. The composite matrix is made of 1050 aluminum alloy, the

Table 2. Chemical and physical properties of HEA type 1.

Fe	Ni	Cr	Co	Ti	Al	Elements
1	1	0.5	1	0.6	0.4	Molar coefficients
22.222	22.222	11.111	22.222	13.333	8.889	Atomic percentage
45	10	63	10	40	20	Particles size (μm)
4.68	4.93	2.17	4.93	2.42	0.87	Weight (g)

Table 3. Chemical and physical properties of HEA type 2.

Fe	Ni	Cr	Co	Mn	Al	Elements
1	1	1	1	1	1.5	Molar coefficients
15.38	15.38	15.38	15.38	15.38	23.10	Atomic percentage
45	10	63	10	63	20	Particles size (μm)
3.48	3.65	3.24	3.68	3.42	2.53	Weight (g)

Table 4. Chemical and physical properties of HEA type 3.

Fe	Ni	Cr	Co	Mn	Elements
1	1	1	1	1	Molar coefficients
20	20	20	20	20	Atomic percentage
45	10	63	10	63	Particles size (μm)
3.98	4.18	3.71	4.21	3.92	Weight (g)

chemical composition of which is given in Table 5. The primary metal powders were prepared from the Pourian Chemical Institute, Iran. Figure 1 shows the size distribution of the HEA particles. The average particle diameter of HEA powders is 21.4 μm.

Mechanical alloying

High entropy alloy particles are produced by mechanical alloying. For this purpose, a planetary ball milling machine (NARYA-MPM 2 × 250 H, Iran) with a rotation speed of 300 rpm and a ball-to-powder ratio of 1:10 was used. Due to the presence of highly active elements, there is a possibility of activation of the materials. An argon gas with a purity of 99% was used to prevent activation of the materials. The size of the balls was determined by trial and error and based on experience. Therefore, balls with diameters of 10, 15 and 20 mm were used for mechanical alloying process. Methanol was also used to prevent the adhesion of powder to balls. As can be seen from Figure 2, after 20 h mechanical alloying, the adhesion of powder particles to balls was not observed. Duration of milling for different alloy compositions was 10, 20 and 30 h. In addition, ARB process was performed at room temperature.

Accumulative roll bonding (ARB)

Before performing the ARB process, the aluminum samples were annealed at 380°C for 2 h. Then, the surface of the cut samples with dimensions of 50 × 100 × 1 mm was thoroughly brushed using a wire brush (Figure 3). Reinforcing particles (4 wt%) were also sprayed on the surface of samples using a 25 micron mesh sieve. Then, two aluminum sheets were tied together using copper wire to prevent them from moving. Then, the distance between the rollers of the rolling machine was set to 1 mm to perform the first rolling pass. After each rolling step, the sample was divided into two parts in the middle and its surface was completely brushed. In order to prevent the formation of bowing defect in the sheet, the rollers were carefully adjusted, and in the next pass, the sample was rotated 180° in the rolling direction. It can be seen in Figure 4(a) that no cracks were formed in the sample after the four rolling passes. However, Figure 4(b) shows that after six rolling passes, cracks were formed on the edges of the sheet. Therefore, the rolling process was carried out in 4 and 6 passes. It should be noted that to achieve uniform distribution of HEA particles within the aluminum matrix, the parameters of the number of rolling passes and the weight percentage of particles are controlled.

The samples were prepared after the ARB process according to Table 6. The input parameters include the weight percentage of high entropy alloy, number of rolling passes, and type of high entropy alloy.

Mechanical tests

Tensile specimens were prepared in the transverse direction of rolling according to the sub size ASTM-E8 standard. Dimensions of tensile specimen were shown in Figure 5. Tensile test was performed with a speed of 1 mm/s at room temperature. A 250 kN Zwick/Roell (Germany) tension machine was used to execute the tensile test. The hardness of the samples was also measured with a Vickers hardness instrument.

Microstructure analysis

In order to investigate the distribution of high-entropy particles, scanning electron microscope (SEM) model FEI-quanta-450 was used. First, the samples were cut in the transverse rolling direction and their cross-sections were examined. The cross-sections of the samples were prepared using sandpaper and polishing. Then, SEM analysis was performed in a vacuum environment with an acceleration voltage of 20 kV. In order to investigate and confirm the formation of solid solution after mechanical alloying, XRD analysis was performed. XRD analysis was also performed to identify the formed elements and the structure of the high entropy alloy. The XRD analysis was performed by a Rigaku Ultima IV X-ray Diffractometer. The average grain size of the samples was calculated using the ImageJ software. The microstructure of samples was also observed by an FEI Talos F200X transmission electron microscopy (TEM).

Results and discussion

XRD analysis

XRD analysis was performed on HEA-type 1 after 5, 10, and 20 h mechanical alloying to confirm the formation of solid

Table 5. Chemical composition of 1050 aluminum alloy.

Elements	Al	Cu	Zn	Fe	Si	Cr	Ti	V
Weight percentage	99.69	0.01	0.02	0.12	0.11	0.01	0.02	0.02

solution, as shown in Figure 6. According to Figure 6, the comparison of X-ray diffraction patterns at different times shows that mechanical alloying is completely performed after 20 h. Moreover, the XRD results show that the produced high entropy structure includes both FCC and BCC crystal structures. It should be noted that this type of high entropy alloy has good ductility due to the presence of FCC structure and high strength due to the presence of BCC structure. The FCC and BCC phases interact with the aluminum matrix during deformation by dislocation pinning as reported in previous research.[81,82] The presence of dislocation pinning was shown by TEM image in Figure 7. High-entropy alloys with FCC structure have more slip planes and lower dislocation density than BCC structure. Hence, the ductility of high-entropy alloys with FCC structure is higher than that of BCC structure.

The XRD analysis results also showed that the intensity of the peaks decreased with increasing milling time, which could be due to the formation of a single solid-state solution. This indicates the formation of a solid solution by dissolution of most of the element in the lattice of Fe or Cr.[83] Moreover, with increasing milling time some amount of peak broadening was observed. This was expected because the increase of milling time decreases the crystallize size and increases the lattice strain[84]. The lattice parameters of the BCC and FCC phases at different milling times were also measured from the XRD pattern, as shown in Figure 6. The lattice parameters of both BCC and FCC phases increase as the milling time prolongs. At the initial stage of milling, the lattice parameters of BCC and FCC phases are rather closed to that of Fe and Ni, respectively. As the mechanical alloying process continues, the simple solid solutions are gradually formed from the principle components. The corporation of elements with larger atomic size, for example Cr and Ti, results in the enlargement in lattice parameter.[85]

Figure 8 shows XRD results for HEA-type 2 after 10 and 20 h mechanical alloying. XRD analysis in Figure 8 shows that after 20 h, mechanical alloying has been well completed. The final structure of HEA-type 2 is BCC, which is consistent with the results obtained in references 86,87. As the milling time increases to 20 h, only peaks belongs to a BCC structure can be identified, by which is deduced the formation of a simple solid solution. The lattice parameters

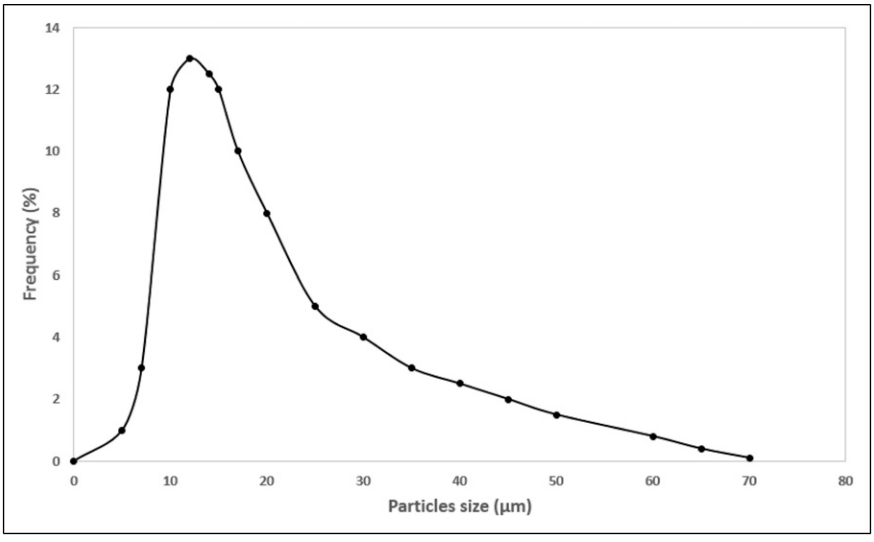

Figure 1. Size distribution of the HEA particles.

Figure 2. Mechanical alloying after 20 hours.

of the BCC phase also increased with increasing milling time.

HEA-type 3 was produced after 30 h mechanical alloying. Figure 9 shows the XRD analysis of HEA-type 3. According to Figure 9, the mechanical alloying was well done and the final crystal structure is FCC. The lattice parameters of the FCC phase also increased with increasing milling time. Throughout the milling process, the decrease

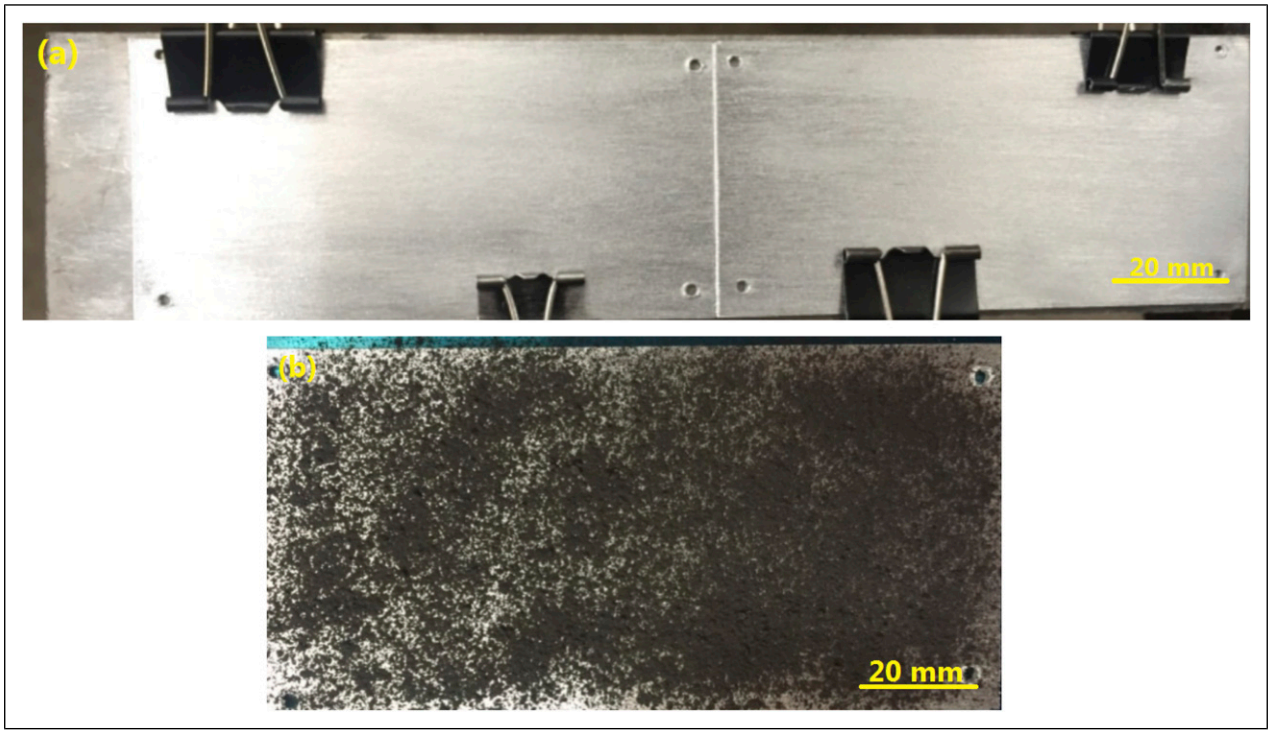

Figure 3. Samples prepared for the ARB process: (a) Brushed samples, (b) particle spraying on the sheet surface.

Figure 4. Rolled samples after (a) 4 rolling passes, (b) 6 rolling passes.

in intensity, broadening of the peak and its subsequent disappearance may result from the three following factors: refined crystal size, high lattice strain and decreased crystallinity.[85]

SEM analysis

Figure 10 shows SEM image of the morphology of the produced high entropy particles. As is clear from Figure 10, these particles do not have a specific and regular shape.

In order to accurately examine the distribution of high entropy particles in the aluminum matrix, SEM images of composite samples produced by the ARB method were observed. Figure 11 shows SEM images of sample ARB144. According to Figure 11, the particle distribution in this sample is almost appropriate, but in some cases there is agglomeration of particles, which results in deterioration of mechanical properties. Agglomeration of HEA particles at 4 wt% was also observed by Luo et al.[88] and Pandey et al.[89] It was detected that the particle size is about 1 μm and less. It should be explained that when HEA particles are uniformly distributed in the composite matrix, the applied load to the matrix is well transferred to the particles and the mechanical properties are improved. In fact, the fine dispersion of HEA particles improves the overall integrity of the composite by providing additional sites for stress transfer.[90–92] However, particle agglomeration prevents the uniform distribution of particles in the matrix, which can lead to deterioration of the mechanical properties of the composite. Also, the agglomeration of HEA particles in the aluminum matrix composite leads to stress concentration and possibly poor bonding between the HEA particles and the aluminum matrix. It should be explained that further increases in HEA content may lead to issues such as particle agglomeration, which can create stress concentrations and act as potential sites for crack initiation.[90–92]

Figure 12 shows SEM images of sample ARB126 at two different magnifications. Figure 12 shows a good particle distribution in sample ARB126, but agglomeration of particles is still observed in some places. It is also observed in Figure 12 that there are very small particle sizes around 30 nm. The SEM images clearly show that the ARB process has been successfully carried out to prepare the composite with high entropy particles. By comparing Figures 11 and

Table 6. Values of parameters for different samples.

Sample number	Type of HEA	Weight percentage of HEA	Number of rolling passes
ARB144	1	4	4
ARB244	2	4	4
ARB344	3	4	4
ARB126	1	2	6
ARB226	2	2	6
ARB326	3	2	6

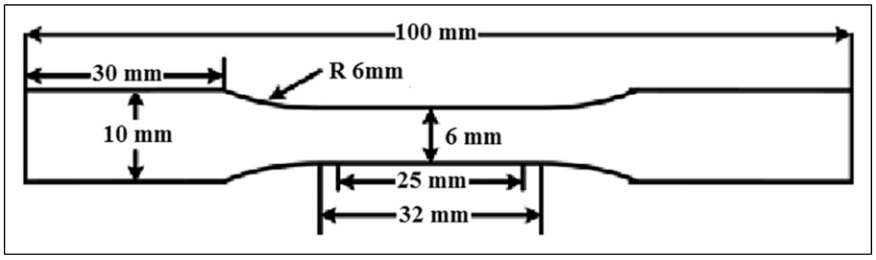

Figure 5. Dimensions of tensile specimen.

12, it can be detected that the distribution of high entropy particles at 2 wt% was more suitable than at 4 wt%, which leads to an improvement in the tensile strength.

Figure 13 shows SEM images of sample ARB244. According to Figure 13, in this sample, defects related to ARB process and severe agglomeration of particles are observed. Agglomerated particles can be susceptible to crack nucleation and growth. In a similar work, Pandey et al.[89] observed that the agglomeration of HEA particles in Al matrix composite produced many cracks on the fractured surface. Moreover, agglomeration of particles prevents uniform distribution of particles within the matrix, which can lead to reduction of the strength of the composite. Huang et al.[93] found that the agglomeration of HEA particles in the Al matrix composite leads to stress concentration and likely poor bonding between HEA particles and Al matrix. Two types of micro-cracks can be formed in the composite structure after the formation of nanoparticle agglomeration. One originates from the inside of agglomerated nanoparticles and propagates towards the aluminum matrix. The other starts from the interface between the agglomerated nanoparticles and the aluminum matrix and then propagates. The formation of the second type of cracks is due to the significant difference in elastic modulus between the HEA particles and the aluminum matrix, which causes a high stress gradient at the interface. It has been reported that if the applied strain rate is not excessive, the propagation of both types of micro-cracks is inhibited by the aluminum matrix.[94]

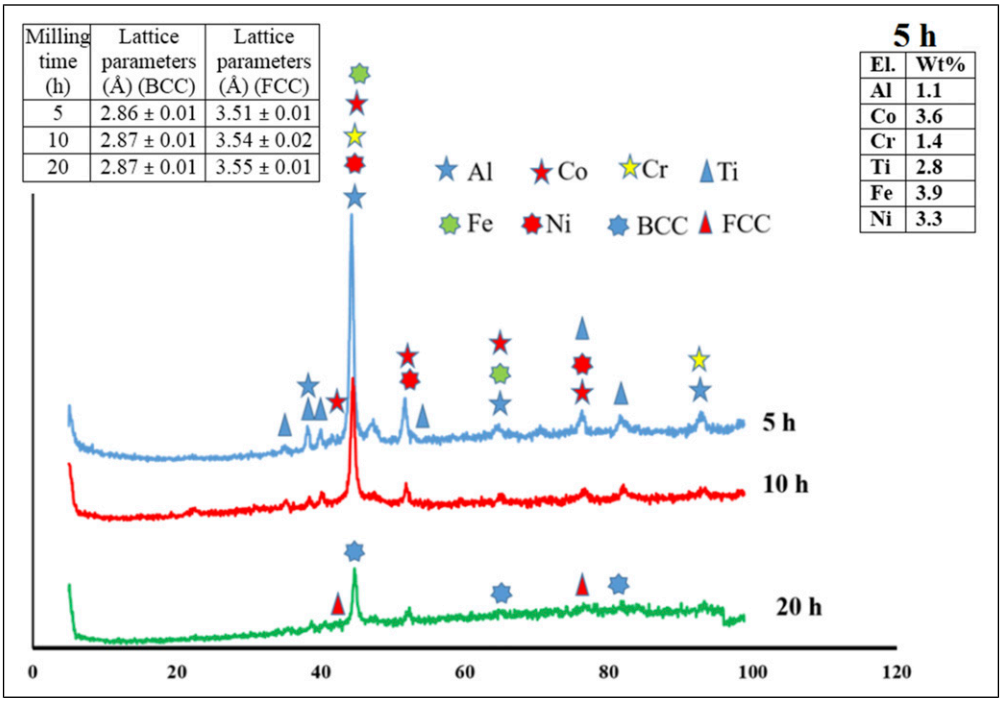

Figure 6. XRD analysis of HEA-type I with chemical composition $Al_{0.4}CoCr_{0.5}NiFeTi_{0.6}$.

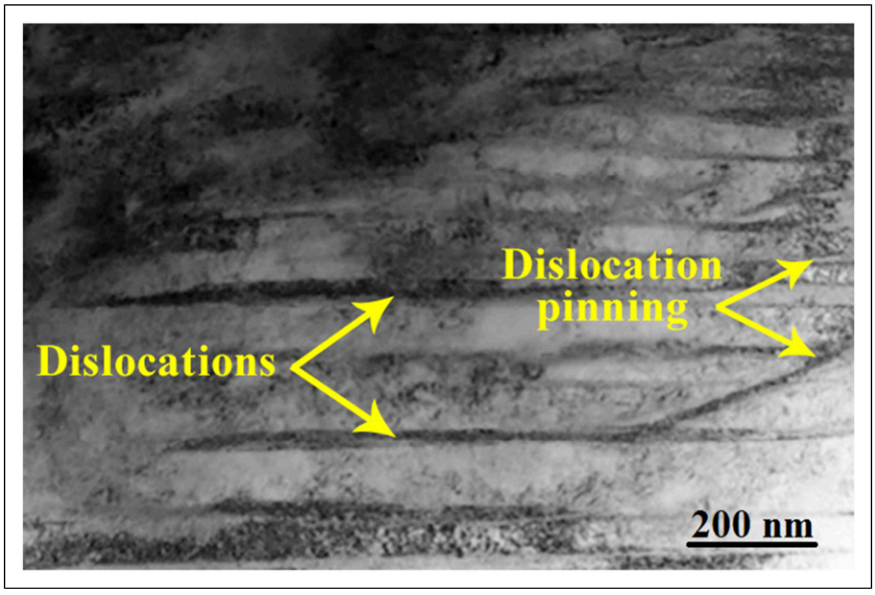

Figure 7. TEM image of dislocation pinning in HEA-type 1.

Figure 14 shows the interface between the HEA particles and the Al matrix. As can be seen from Figure 14, in all samples a good bond was formed between the HEA particles and the AL matrix. However, in samples where particle agglomeration occurred, cracks were observed between the particles and the AL matrix (Figure 14(c)).

Figure 15 shows SEM images of sample ARB326. The particle size has been measured to be about 50 nm. Figure 15

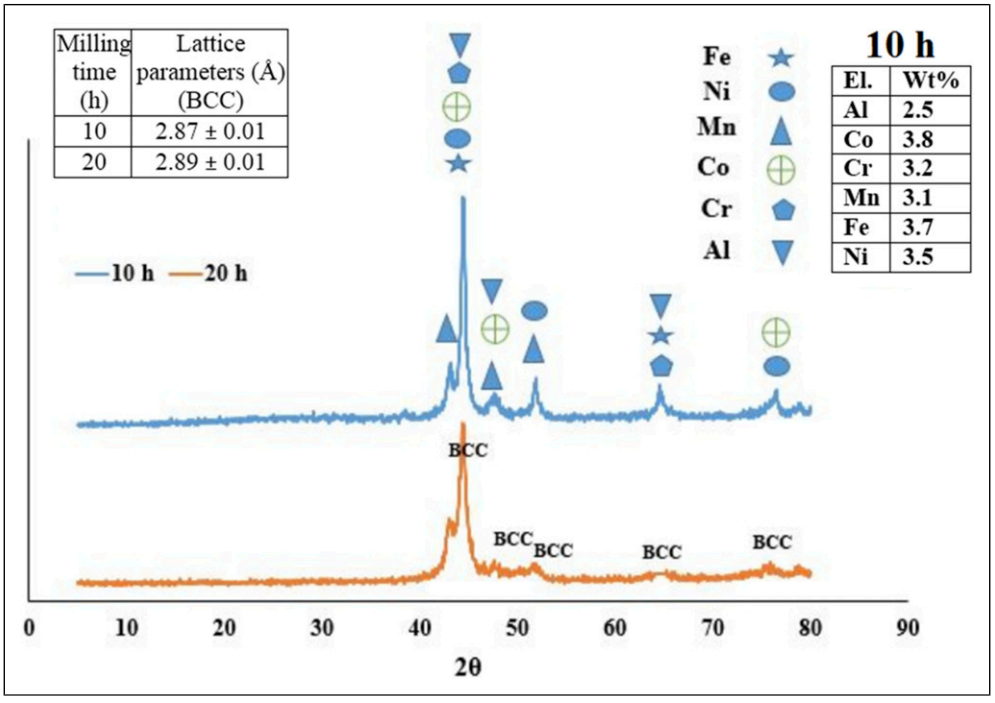

Figure 8. XRD analysis of HEA-type 2 with chemical composition $Al_{1.5}MnCoCrNiFe$.

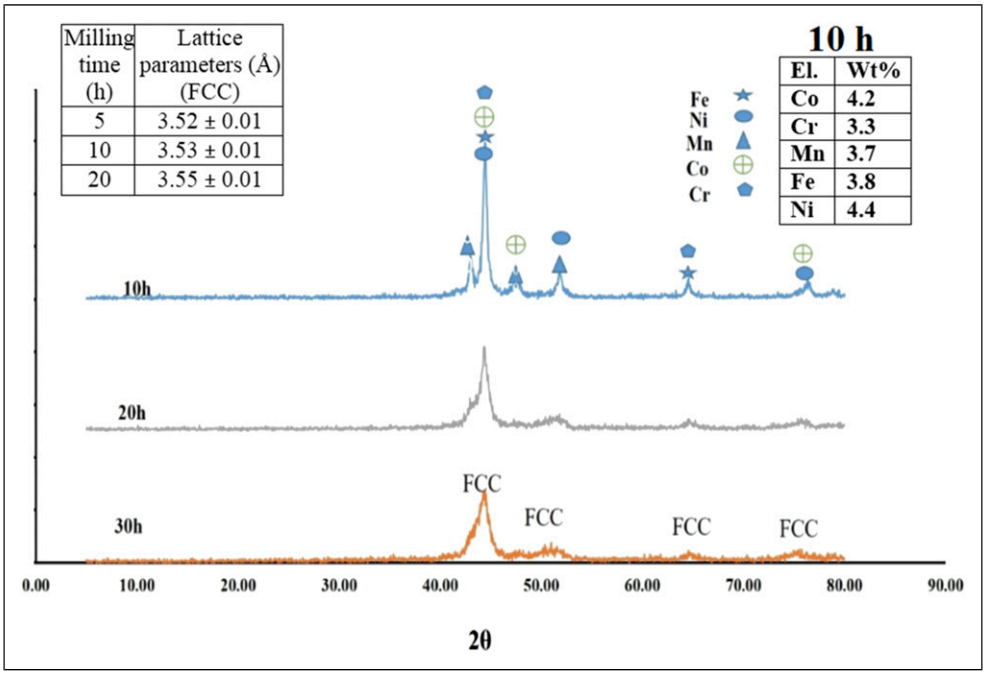

Figure 9. XRD analysis of HEA-type 3 with chemical composition MnCoCrNiFe.

shows that the particle distribution is appropriate, but micro-cracks are visible at higher magnification, which reduce the ultimate strength of the composite. The presence of micro-cracks in the microstructure is due to the increased number of rolling passes. In general, the SEM images indicated that a good particle distribution was obtained in the samples produced by 2 wt% HEA after six rolling passes. However, in the samples produced by 4 wt% HEA, agglomeration of particles was observed.

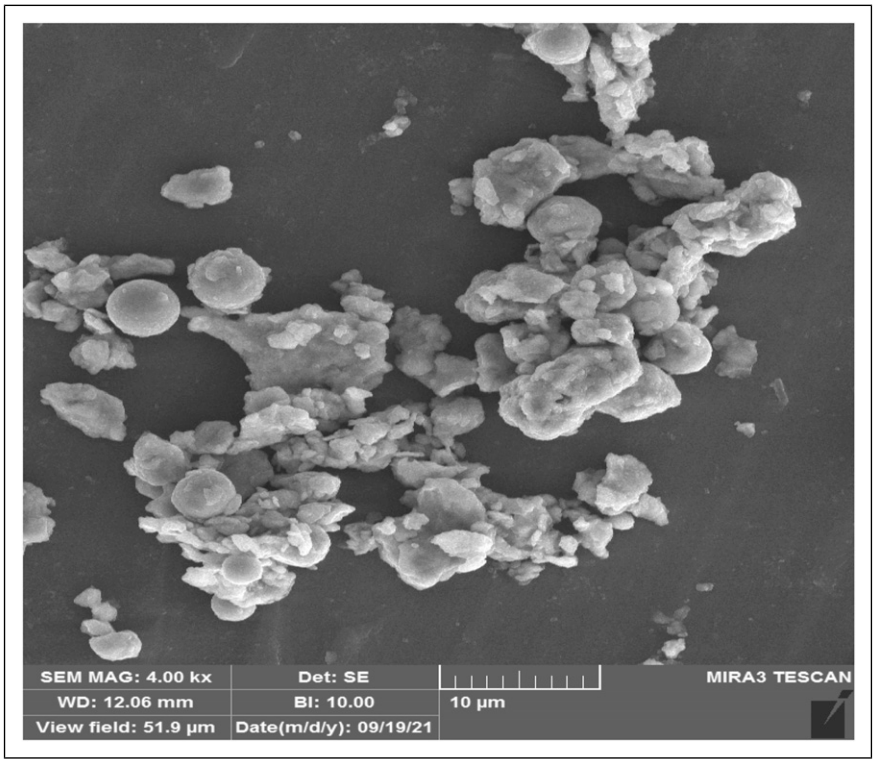

Figure 10. SEM image of the morphology of the produced high entropy particles.

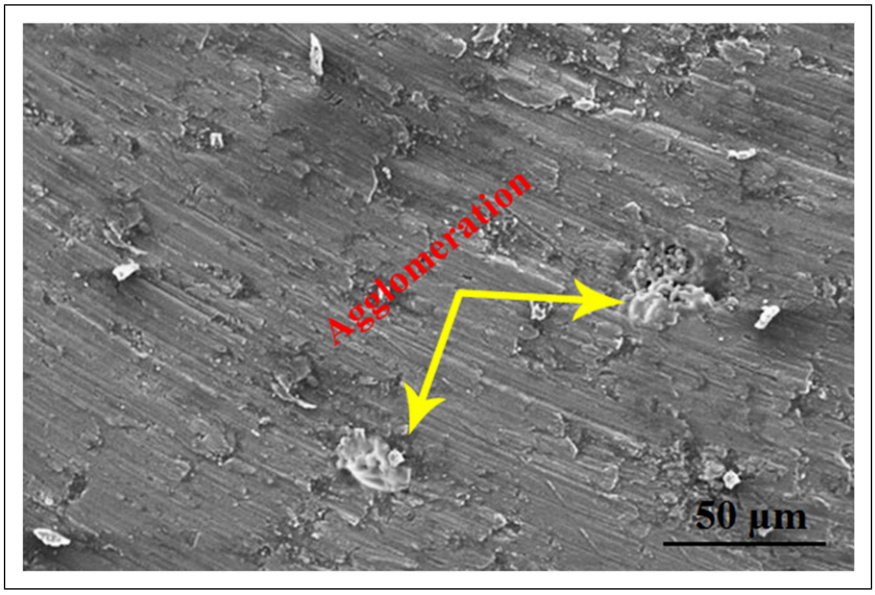

Figure 11. SEM image of sample ARB144.

The results of this study indicated that by changing the process parameters, the agglomeration of nanoparticles can be prevented. For example, by increasing the number of rolling passes, the distribution of nanoparticles is improved. However, increasing the number of passes to 6 passes causes cracks in the microstructure of the composite. It has been reported that the agglomeration of nanoparticles can also be reduced by the surface treatment of the HEA using different

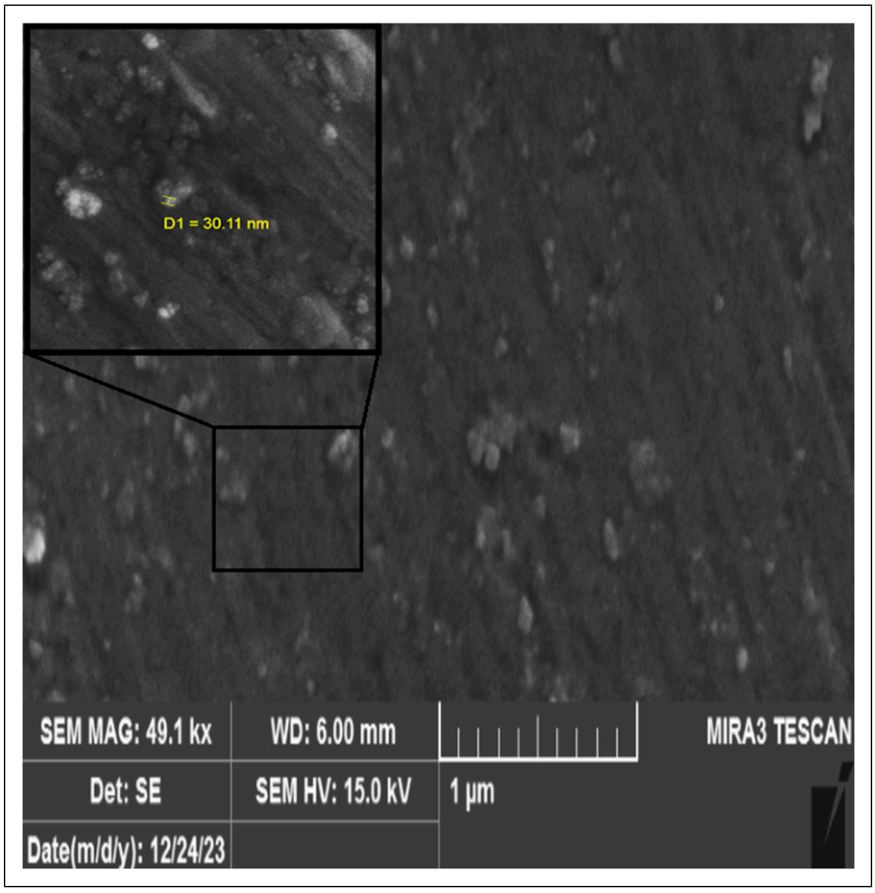

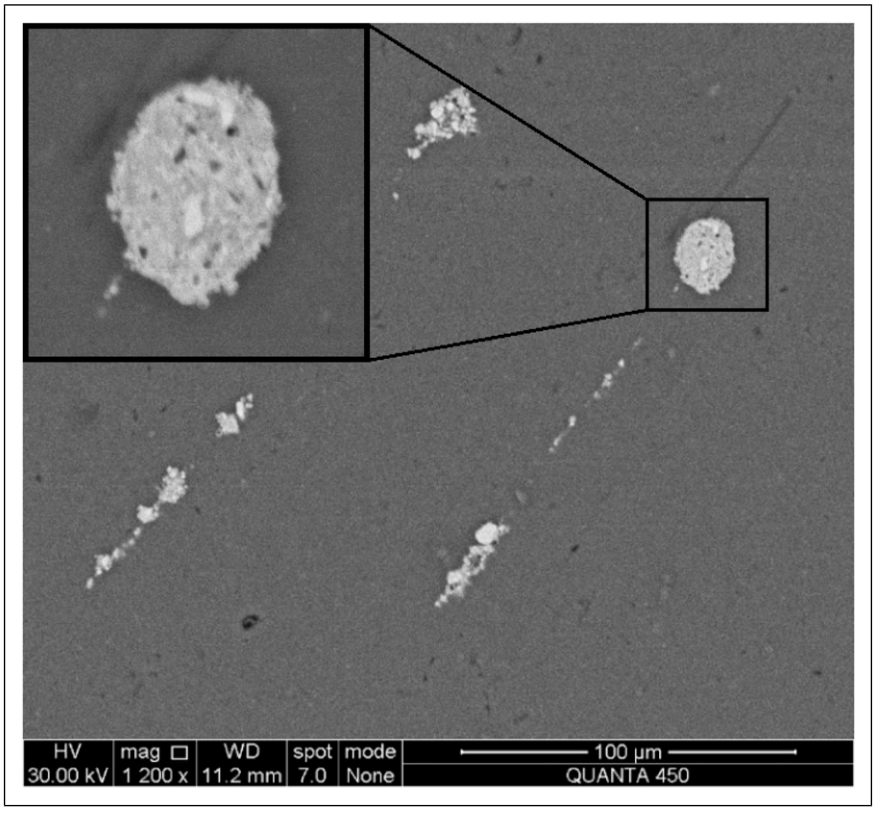

Figure 13. SEM image of sample ARB244.

methods such as electron beams and high-temperature pulsed plasma flows.[95,96]

The microstructure of the ARB samples after each rolling pass is shown in Figure 16. Moreover, Figure 17 shows the effect of rolling passes on the grain size. It can be observed from Figure 17 that the grain size of microstructure for 0, 2, 4 and 6 rolling passes is 34, 16, 9 and 6 µm, respectively. Microstructural changes during the ARB process are usually controlled by the stacking fault energy of material. The development of fine-grained microstructure in the ARBed Al as a high stacking fault energy metal can be explained as follows.[97] The early ARB cycles are accompanied by increasing density of dislocations and subsequent interactions. Increasing the strain results in the development of 3D dislocation arrays, such as sub-grains, spreading throughout the coarse-grained sample. The increase in the ARB cycles is followed by formation of finer grains. Further strain leads to the failure of the initial coarse grains and the formation of

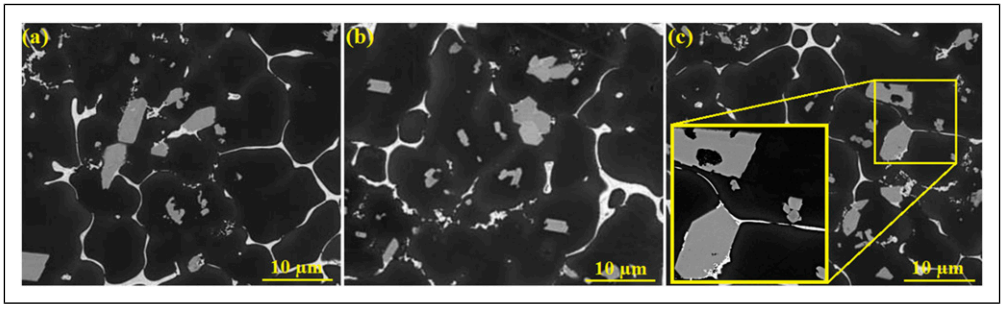

Figure 14. SEM image of samples (a) ARB126, (b) ARB244, (c) ARB326.

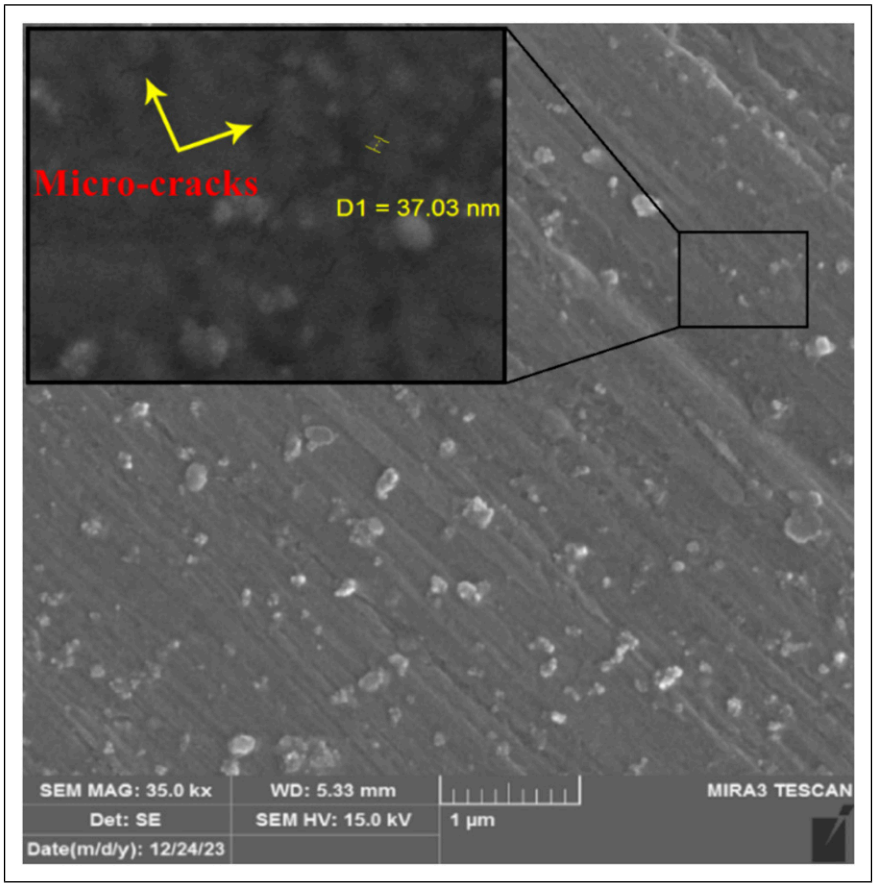

Figure 15. SEM image of sample ARB326.

new grain boundaries, ultimately resulting in fine-grained microstructure.

Mechanical properties

The results of measuring the tensile strength, elongation, hardness and agglomeration percentage of the composites prepared using ARB are presented in Table 7. Each experiment was repeated twice (12 samples) and the error of each experiment is given in Table 7. The results of measuring the tensile strength, elongation, and hardness of the composites were also shown in Figure 18. It can be seen from Table 7 and Figure 18 that the highest tensile strength and elongation were obtained for sample ARB126. Therefore, the elongation and tensile strength simultaneously increased in this sample. It can be therefore concluded that by using high entropy particles of $Al_{0.4}Ti_{0.6}CoCr_{0.5}NiFe$, tensile strength and elongation are simultaneously improved due to the presence of both FCC and BCC structures. In fact, the FCC structure of HEA-type 1 improved the ductility, and BCC structure improved the strength of the composite. Simultaneous improvement of tensile strength and elongation by addition of HEA particles to Al matrix composites was also observed by Tan et al.[53] Zhang et al.[62] Li et al.[70] and Luo et al.[88] However, Table 7 shows that the highest hardness was obtained for sample ARB244, due to formation of BCC structure in the high entropy particles of $Al_{1.5}MnCoCrNiFe$ (HEA-type 2). Moreover, samples prepared from HEA-type 2 particles are more suitable in terms of strength, hardness and elongation than samples prepared from HEA-type 3.

The results of Table 7 also showed that increasing the amount of reinforcement caused a decrease in tensile strength and elongation. As can observed from the SEM images (Figures 11 and 13), with increasing the amount of reinforcement, agglomeration of particles occurred, which caused the initiation and propagation of cracks, and consequently decreased the tensile strength and elongation of the composite. However, increasing the amount of HEA particles improved the hardness of the composite because the hardness of HEA particles was higher compared to the aluminum matrix. In a similar study, An et al.[98] reported that the increase of HEA particles in the Al matrix composite improved the

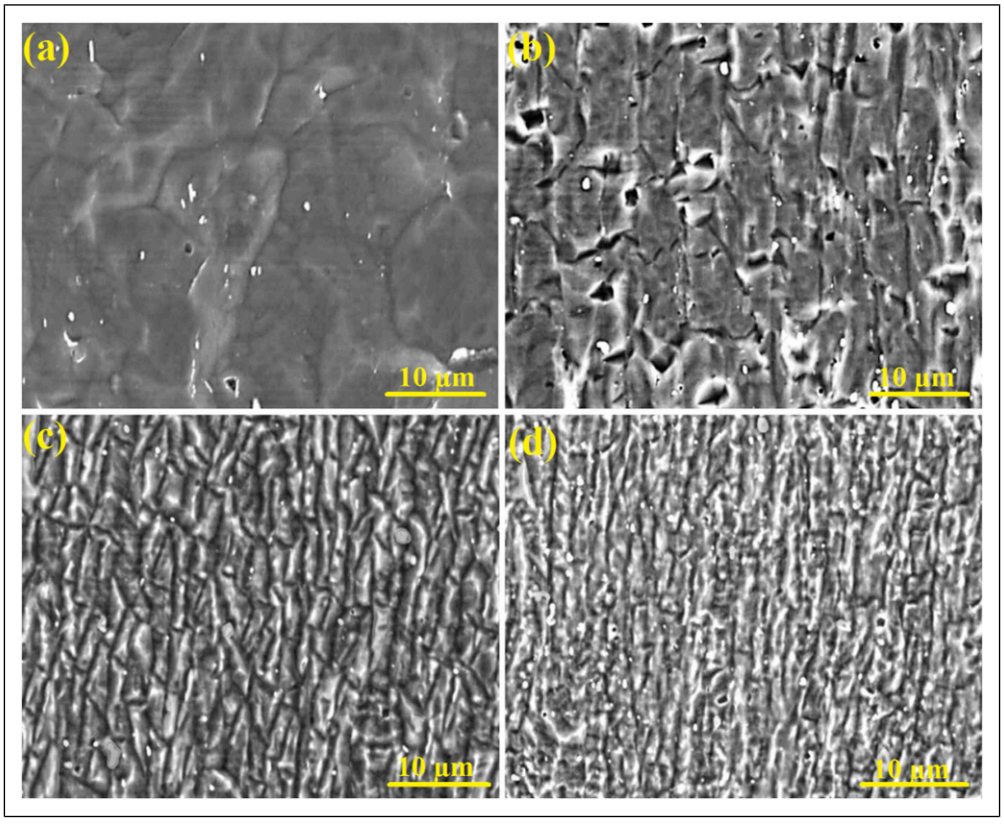

Figure 16. SEM image of ARB samples after (a) 0, (b) 2, (c) 4, (d) 6 rolling pass.

hardness, but reduced the strength of the composite. The amount of agglomerated nanoparticles under different parameter conditions was quantified using ImageJ software, as shown in Table 7. The agglomeration percentage was calculated by surface area percentage. According to the maximum particle size (70 µm), the minimum surface area that leads to agglomeration was estimated and the surface area percentage was calculated.

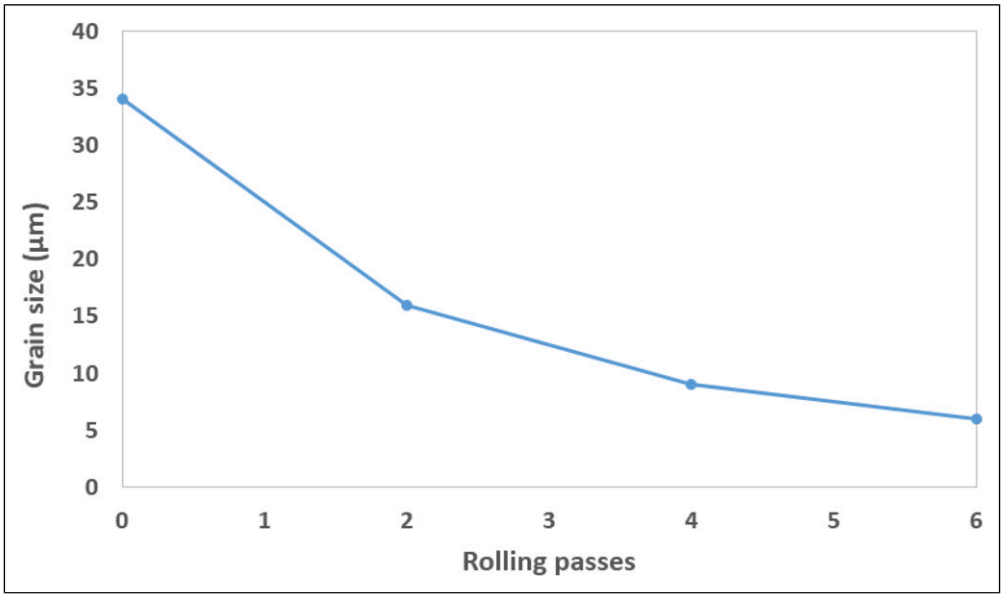

Figure 17. Effect of rolling passes on grain size.

Table 7. Results of measuring the tensile strength, elongation, and hardness.

Samples	Type of HEA	Weight percentage of HEA	Number of rolling passes	Elongation (%)	Tensile strength (MPa)	Hardness (HV)	Agglomeration percentage
ARB144	1	4	4	1.87 ± 0.1	178.5 ± 2	38.2 ± 0.6	2.4
ARB244	2	4	4	1.84 ± 0.1	182 ± 3	39.9 ± 0.7	2.1
ARB344	3	4	4	2.96 ± 0.2	175 ± 1	36.9 ± 0.5	2.9
ARB126	1	2	6	3.44 ± 0.2	202.5 ± 3	28.3 ± 0.5	0.6
ARB226	2	2	6	2.14 ± 0.1	190 ± 3	38.8 ± 0.4	0.4
ARB326	3	2	6	1.3 ± 0.1	169.5 ± 2	35.2 ± 0.6	0.7

It can also be seen from Table 7 that increasing the number of rolling passes has increased the tensile strength and elongation. The most important reason for improvement of the mechanical properties of the composite is that with increasing the number of rolling passes, the distribution of HEA particles in the Al matrix improved. Another reason for the improvement of mechanical properties due to the increase in the number of rolling passes is the refinement of the microstructure. As the grain size decreases, the grain boundaries increase, leading to an increase in dislocation density, because the obstacles to dislocation movement increase. An increase in the dislocation density leads to an improvement in the tensile strength However, it should be noted that the number of rolling passes is lower in samples with a higher percentage of HEA particles because in samples with a higher percentage of HEA particles, cracks are created in fewer passes. In general, the results showed that cracks usually started to appear after six rolling passes. However, in the samples with a higher percentage of HEA particles (4 wt %), cracks appeared after 4 passes. Therefore, the critical number of rolling passes at which cracking becomes a

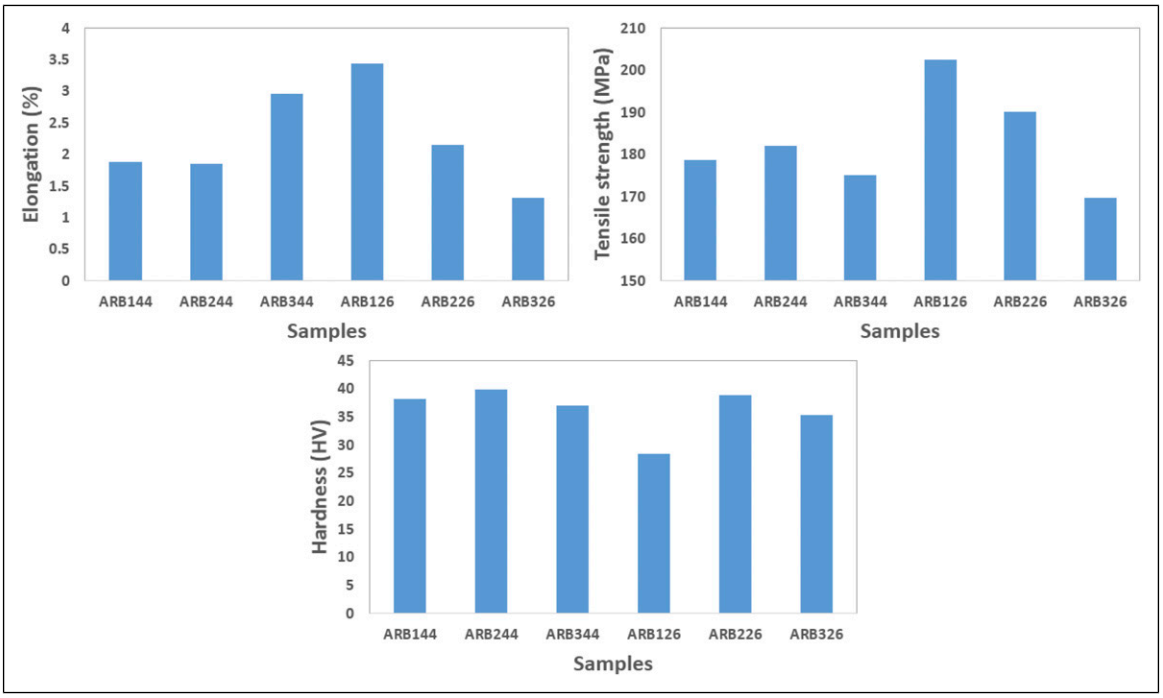

Figure 18. Results of measuring the tensile strength, elongation, and hardness.

significant concern is 6 and 4 passes for the samples with 2 and 4 wt% HEA, respectively.

Conclusion

In this paper, accumulative roll bonding (ARB) process is used to produce aluminum matrix composite reinforced by high entropy alloy (HEA) and achieve a suitable combination of strength and ductility. The results were summarized as follows:

(1) A good particle distribution was obtained in the samples produced by 2 wt% HEA after six rolling passes. However, in the samples produced by 4 wt% HEA, agglomeration of particles was observed.
(2) By using HEA particles of $Al_{0.4}Ti_{0.6}CoCr_{0.5}NiFe$, tensile strength and elongation are simultaneously improved by 4% and 58% respectively, due to the presence of both FCC and BCC structures. However, the highest hardness of 39.9 HV was obtained for sample prepared by HEA particles of $Al_{1.5}$MnCoCrNiFe, due to formation of BCC structure.
(3) With increasing the amount of reinforcement up to 4 wt%, agglomeration of particles occurred, which caused the initiation and propagation of cracks, and consequently decreased the tensile strength and elongation of the composite by about 54% and 12% respectively.
(4) The increase of the number of rolling passes from 4 to 6 increased the tensile strength and elongation by 84% and 13% respectively, because the distribution of HEA particles in the Al matrix improved.
(5) The highest tensile strength (202.5 MPa) and elongation (3.44%) were obtained for the sample produced with 2 wt% $Al_{0.4}CoCr_{0.5}NiFeTi_{0.6}$ at six rolling passes. However, the highest hardness was obtained for sample produced with 4 wt% $Al_{1.5}$MnCoCrNiFe (39.9 HV).
(6) Due to the simultaneous increase in tensile strength and elongation, the produced composite sample can be used in the automotive and aerospace industries. However, it should be noted that due to the layered structure of the sheet after the ARB process, the wear resistance of the sample decreases.[99] Wear resistance of the produced samples after the ARB process can be enhanced by performing heat treatments or coating process.[100,101]

ORCID iD

Mohsen Haddad Sabzevar https://orcid.org/0009-0002-7263-6932

Funding

The authors received no financial support for the research, authorship, and/or publication of this article.

Declaration of conflicting of interests

The authors declared no potential conflicts of interest with respect to the research, authorship, and/or publication of this article.

Data Availability Statement

The authors confirm that the data supporting the findings of this study are available within the article.

References

1. Xu S, Jing X, Zhu P, et al. Equilibrium phase diagram design and structural optimization of SAC/Sn-Pb composite structure solder joint for preferable stress distribution. *Mater Char* 2023; 206: 113389.
2. Liu J, Xu J, Paik K-W, et al. In-situ isothermal aging TEM analysis of a micro Cu/ENIG/Sn solder joint for flexible interconnects. *J Mater Sci Technol* 2024; 169: 42–52.
3. Ji R, Zhao Q, Zhao L, et al. Study on high wear resistance surface texture of electrical discharge machining based on a new water-in-oil working fluid. *Tribol Int* 2023; 180: 108218.
4. Ji R, Liu Y, Zhang Y, et al. Machining performance of silicon carbide ceramic in end electric discharge milling. *Int J Refract Metals Hard Mater* 2011; 29(1): 117–122.
5. Ji R, Liu Y, Zhang Y, et al. Influence of dielectric and machining parameters on the process performance for electric discharge milling of SiC ceramic. *Int J Adv Manuf Technol* 2012; 59: 127–136.
6. Li R, Ju G, Zhao X, et al. Simulation of residual stress and distortion evolution in dual-robot collaborative wire-arc additive manufactured Al-Cu alloys. *Virtual Phys Prototyp* 2024; 19(1): e2409390.
7. Li B, Jiang S-D, Fu Q, et al. Tailoring Nanocrystalline/Amorphous Interfaces to Enhance Oxygen Evolution Reaction Performance for FeNi-Based Alloy Fibers. *Adv Funct Mater* 2025; 35(2): 2413088.
8. Wang J, Xie Y, Meng X, et al. Wire-based friction stir additive manufacturing towards isotropic high-strength-ductility Al-Mg alloys. *Virtual Phys Prototyp* 2024; 19(1): e2417369.
9. Hu Z, Zheng J, Hua L, et al. Investigation of forging formability, microstructures and mechanical properties of pre-hardening Al-Zn-Mg-Cu alloy. *J Manuf Process* 2024; 131: 2082–2100.
10. Fan T, Ruan Z, Zhong F, et al. Nucleation and growth of L12-Al3RE particles in aluminum alloys: a first-principles study. *J Rare Earths* 2023; 41(7): 1116–1126.
11. Altinkok N. Microstructure and tensile strength properties of aluminium alloys composites produced by pressure-assisted aluminium infiltration of Al_2O_3/SiC preforms. *J Compos Mater* 2004; 38: 1533–1543.
12. Li W, Xie D, Li D, et al. Mechanical behavior of high-entropy alloys. *Prog Mater Sci* 2021; 118: 100777.
13. Smirnov AS, Shveikin VP, Smirnova EO, et al. Effect of silicon carbide particles on the mechanical and plastic

properties of the AlMg6/10% SiC metal matrix composite. *J Compos Mater* 2018; 52: 3351–3363.
14. Huang M, Wang L, Wang C, et al. Optimizing crack initiation energy in austenitic steel via controlled martensitic transformation. *J Mater Sci Technol* 2024; 198: 231–242.
15. Wang F, Liu Y, Yu W, et al. Effect of electropulsing treatment on the microstructure and mechanical properties of Ti6Al4V alloy processed by a hybrid method of directed energy deposition and layer-by-layer ultrasonic impact peening. *Mater Sci Eng, A* 2024; 908: 146774.
16. Chi Y, Dong Z, Cui M, et al. Comparative study on machinability and surface integrity of γ-TiAl alloy in laser assisted milling. *J Mater Res Technol* 2024; 33: 3743–3755.
17. Fang Z, Ma B, Liang E, et al. Interaction regularity of biomolecules on Mg and Mg-based alloy surfaces: a first-principles study. *Coatings* 2023; 14(1): 25.
18. Xin M, Fan Z, Lu L, et al. Surface enhancement of metallic alloys by laser precision engineering. *Weld World* 2024; 68(11): 3033–3050.
19. Wang Z, Ning Y, Di P, et al. Understanding the fracture mechanisms of Ni–Co–Cr-type superalloys: role of precipitate evolution and strength degradation. *Mater Sci Eng, A* 2024; 902: 146623.
20. Yu W, Chong X, Liang Y, et al. Discovering novel γ-γ' Pt-Al superalloys via lattice stability in Pt3Al induced by local atomic environment distortion. *Acta Mater* 2024; 281: 120413.
21. Qu X, Li X, Zhang L, et al. Effect of construction angles on the microstructure and mechanical properties of LPBF-fabricated 15-5 PH stainless steel. *Mater Sci Eng, A* 2024; 900: 146423.
22. Fu J, Zhang L, Wang H, et al. Microstructure and mechanical properties of WC-12Co cemented carbide fabricated by laser powder bed fusion on a WC-20Co cemented carbide substrate. *J Mater Res Technol* 2024; 30: 9093–9101.
23. Phung-Van P, Nguyen-Xuan H, Hung PT, et al. Nonlocal strain gradient analysis of honeycomb sandwich nanoscale plates. *Thin-Walled Struct* 2024; 198: 111746.
24. Jackson A, Davidson P and Adnan A Low velocity impact resistance of multilayer composite structures for mitigating acceleration. *J Compos Mater* 2025; 59: 383–393.
25. Liu X, He D, Zhu B, et al. The ordered orientation gradient "sandwich" texture induced high strength-ductility in AZ31 magnesium alloy. *Scr Mater* 2024; 253: 116296.
26. Guo X, Tian D, Li C, et al. Optimization for the process parameters of nickel–titanium nitride composites fabricated via jet pulse electrodeposition. *Nanomaterials* 2024; 14(24): 2034.
27. Long X, Su T, Lu C, et al. An insight into dynamic properties of SAC305 lead-free solder under high strain rates and high temperatures. *Int J Impact Eng* 2023; 175: 104542.
28. Chen X, Xia D, Jia Q, et al. Significantly improve the strength and ductility of AZ31 Mg alloy by introducing pure Ti. *J Mater Sci Technol* 2024; 185: 69–82.
29. Chen X, Zhang J, Wang M, et al. Research progress of heterogeneous structure magnesium alloys: a review. *J Magnesium Alloys* 2024; 12(6): 2147–2181.
30. Sun Y, Chen Y, Tsuji N, et al. Microstructural evolution and mechanical properties of nanostructured Cu/Ni multilayer fabricated by accumulative roll bonding. *J Alloys Compd* 2020; 819: 152956.
31. Ebrahimi M and Wang Q. Accumulative roll-bonding of aluminum alloys and composites: an overview of properties and performance. *J Mater Res Technol* 2022; 19: 4381–4403.
32. Long X, Chong K, Su Y, et al. Connecting the macroscopic and mesoscopic properties of sintered silver nanoparticles by crystal plasticity finite element method. *Eng Fract Mech* 2023; 281: 109137.
33. Fathy A, Ibrahim D, Elkady O, et al. Evaluation of mechanical properties of 1050-Al reinforced with SiC particles via accumulative roll bonding process. *J Compos Mater* 2019; 53: 209–218.
34. Meselhy A and Reda M. Investigation of mechanical properties of nanostructured Al-SiC composite manufactured by accumulative roll bonding. *J Compos Mater* 2019; 53: 3951–3961.
35. Mitsuyuki Cintho O, Luiz Sordi V and Kliauga A; Danielle Cristina Camilo Magalhães. Improved tensile properties in heterostructured 1050/7050 Al sheets produced by accumulative roll bonding. *J Mater Res Technol* 2022; 17: 2014–2025.
36. Huot J. *Enhancing hydrogen storage properties of metal hybrides: enhancement by mechanical deformations*. Springer, 2016.
37. Elwan M, Fathy A, Wagih A, et al. Fabrication and investigation on the properties of ilmenite ($FeTiO_3$)-based Al composite by accumulative roll bonding. *J Compos Mater* 2020; 54: 1259–1271.
38. Gholami MD, Salamat M and Hashemi R. Study of mechanical properties and wear resistance of Al 1050/Brass (70/30)/Al 1050 composite sheets fabricated by the accumulative roll bonding process. *J Manuf Process* 2021; 71: 407–416.
39. GholamiHashemiSedighi MDRM and Sedighi M. The effect of temperature on the mechanical properties and forming limit diagram of aluminum strips fabricated by accumulative roll bonding process. *J Mater Res Technol* 2020; 9(2): 1831–1846.
40. Najjar IR and Elmahdy M. Study of mechanical properties and wear resistance of nanostructured Al 1100/TiO_2 nanocomposite processed by accumulative roll bonding. *J Compos Mater* 2022; 56: 2727–2738.
41. Chekhonin P, Beausir B, Scharnweber J, et al. Confined recrystallization of high-purity aluminium during accumulative roll bonding of aluminium laminates. *Acta Mater* 2012; 60: 4661–4671.
42. Vini MH, Daneshmand S and Forooghi M. Roll bonding properties of Al/Cu bimetallic laminates fabricated by the roll bonding technique. *Technologies* 2017; 5(2): 32.

43. Vini MH and Daneshmand S. Investigation of bonding properties of Al/Cu bimetallic laminates fabricated by the asymmetric roll bonding techniques. *Advances in computational design* 2019; 4(1): 33–41.
44. Saade Abdalkareem J, Vini MH and Daneshmand S. Bonding properties of Al/Al_2O_3 bulk composites produced via combined stir casting and accumulative press bonding. *Surf Rev Lett* 2022; 29(04): 2250052.
45. Sajjadi Nikoo S, Kumaran SN, Qods F, et al. Microstructure evolution and mechanical properties of the AA2024/AA5083 ultra-fine grained composite fabricated via accumulative roll bonding (ARB) method. *J Mater Res* 2023; 38(9): 2519–2533.
46. Liu W, Ke Y, Sugio K, et al. Microstructure and mechanical properties of Al_2O_3-particle-reinforced Al-matrix composite sheets produced by accumulative roll bonding (ARB). *Mater Sci Eng, A* 2022; 850: 143574.
47. Roghani H, Borhani E, Shams SAA, et al. On the microstructure, texture and mechanical properties through heat treatment in Al–CuO nanocomposite fabricated by Accumulative Roll Bonding (ARB). *Mater Sci Eng, A* 2021; 828: 142080.
48. Ramkumar KR, Dinaharan I, Murugan N, et al. Development of aluminum matrix composites through accumulative roll bonding: a review. *J Mater Sci* 2024; 59: 8606–8649.
49. Ujah CO, Popoola PA, Popoola O, et al. Mechanical and thermal behaviors of Ti36-Al16-V16-Fe16-Cr16 high entropy alloys fabricated by spark plasma sintering: an advanced material for high temperature/strength applications. *J Compos Mater* 2022; 56: 3913–3923.
50. Pandian V and Kannan S. Influence of CrCuFeMnNi high entropy alloy particle on the microstructure and mechanical properties of aerospace-grade aluminum 7075 metal-metal composite. *Proc IME C J Mech Eng Sci* 2024; 238: 8274–8293.
51. Li C, Zheng Y, Wang Y, et al. Interfacial microstructure evolution and bonding mechanism transformation of CoCrFeMnNi high-entropy alloy joints fabricated by vacuum hot-compression bonding. *J Mater Res Technol* 2023; 25: 2717–2737.
52. Pandian V and Kannan S. High-entropy alloy reinforcement in aerospace-grade aluminum 7075: a study of yield strength and elastic modulus. *Proc IME C J Mech Eng Sci* 2024; 238: 5043–5063.
53. Tan Z, Wang L, Xue Y, et al. High-entropy alloy particle reinforced Al-based amorphous alloy composite with ultrahigh strength prepared by spark plasma sintering. *Mater Des* 2016; 109: 219–226.
54. Lu T, He T, Li Z, et al. Microstructure, mechanical properties and machinability of particulate reinforced Al matrix composites: a comparative study between SiC particles and high-entropy alloy particles. *J Mater Res Technol* 2020; 9: 13646–13660.
55. Wang W, Zhao W, Mu W, et al. Effect of hot-rolling process on the microstructure, mechanical and corrosion behaviors of dual-phase Co-based entropic alloys. *Mater Sci Eng, A* 2024; 918: 147433.
56. Yang ML, Xu JL, Huang J, et al. Wear resistance of N-doped CoCrFeNiMn high entropy alloy coating on the Ti-6Al-4V alloy. *J Therm Spray Technol* 2024; 33: 2408–2418.
57. Geng Z, Chen C, Song M, et al. High strength $Al_{0.7}$CoCrFeNi$_{2.4}$ hypereutectic high entropy alloy fabricated by laser powder bed fusion via triple-nanoprecipitation. *J Mater Sci Technol* 2024; 187: 141–155.
58. Cui M, Zhang T, Ni J, et al. First-principles study on the hydrogen embrittlement resistance of CoCrFeMnNi high-entropy alloys. *Int J Hydrogen Energy* 2025; 106: 1275–1284.
59. Fu A, Xie Z, Wang J, et al. Controlling of cellular substructure and its effect on mechanical properties of FeCoCrNiMo$_{0.2}$ high entropy alloy fabricated by selective laser melting. *Mater Sci Eng, A* 2024; 901: 146547.
60. Xu X, Song Z, Wang K, et al. Cryo-rolling and annealing-mediated phase transformation in $Al_5Ti_{2.5}Fe_{25}Cr_{25}Ni_{42.5}$ high-entropy alloy: experimental, phase-field and CALPHAD investigation. *J Mater Sci Technol* 2025; 219: 307–325.
61. Guo Q, Hou H, Wang K, et al. Coalescence of $Al_{0.3}$CoCrFeNi polycrystalline high-entropy alloy in hot-pressed sintering: a molecular dynamics and phase-field study. *Npj Comput Mater* 2023; 9(1): 185.
62. Zhang F, He Z, Lu K, et al. Interfacial microstructure and mechanical properties of 2124 aluminum alloy reinforced by AlCoCrFeNi high entropy alloy. *J Mater Res Technol* 2023; 26: 8846–8856.
63. Yuan Z, Tian W, Li F, et al. Microstructure and properties of high-entropy alloy reinforced aluminum matrix composites by spark plasma sintering. *J Alloys Compd* 2019; 806: 901–908.
64. Zhu R, Sun Y, Feng J, et al. Effect of microstructure on mechanical properties of FeCoNiCrAl high entropy alloys particle reinforced Cu matrix surface composite prepared by FSP. *J Mater Res Technol* 2023; 27: 2695–2708.
65. Xiang T, Du P, Bao W, et al. Bimodal grain size structure design to optimize the mechanical properties of TiZrNbTa high entropy alloys/Ti composites. *Mater Sci Eng, A* 2022; 849: 143488.
66. Luo K-G, Wu Y-G, Xiong H-Q, et al. Enhanced mechanical properties of aluminum matrix composites reinforced with high-entropy alloy particles via asymmetric cryorolling. *Trans Nonferrous Metals Soc China* 2023; 33(7): 1988–2000.
67. Wang E, Lv L, Kang F, et al. Microstructure and bending behavior of Ti/Al laminated composites reinforced with high-entropy alloy particles. *J Mater Res Technol* 2023; 27: 7495–7505.
68. Liu C, Jiang X, Sun H, et al. Microstructure and mechanical properties of bioinspired laminated CoCrFeNiMn high entropy alloy matrix composites reinforced with graphene. *Mater Sci Eng, A* 2022; 859: 144198.

69. Seenivasan S, Soorya Prakash K, Nandhakumar S, et al. Influence of AlCoCrCuFe high entropy alloy particles on the microstructural, mechanical and tribological properties of copper surface composite made through friction stir processing. *Proc IME C J Mech Eng Sci* 2021; 235: 5555–5566.
70. Emamifar A, Sadeghi B, Cavaliere P, et al. Microstructural evolution and mechanical properties of AlCrFeNiCoC high entropy alloy produced via spark plasma sintering. *Powder Metall* 2019; 62(1): 61–70.
71. Zhang G, Yang X, Zhao Y, et al. Microstructure and mechanical properties regulation and control of in-situ TiC reinforced CoCrFeNiAl0.2 high-entropy alloy matrix composites via high-gravity combustion route. *J Alloys Compd* 2022; 899: 163221.
72. Konovalov S, Gudala S, Panchenko I, et al. Evolution of microstructure, mechanical properties and phase stability of CoCrFeMnNi high entropy alloys. *Vacuum* 2024; 227: 113405.
73. Luo W, Yuan X, Zhang Z, et al. Effect of volumetric energy density on the mechanical properties and corrosion resistance of laser-additive-manufactured $AlCoCrFeNi_{2.1}$ high-entropy alloys. *J Alloys Compd* 2025; 1010: 178032.
74. Shadangi Y, Chattopadhyay K and Mukhopadhyay NK. Powder metallurgical processing of Al matrix composite reinforced with AlSiCrMnFeNiCu high-entropy alloys: microstructure, thermal stability, and microhardness. *J Mater Res* 2023; 38(1): 248–264.
75. Sathiyamoorthi P, Basu J, Kashyap S, et al. Thermal stability and grain boundary strengthening in ultrafine-grained CoCrFeNi high entropy alloy composite. *Mater Des* 2017; 134: 426–433.
76. Jadhav MS, Sahane D, Verma A, et al. Thermal stability and thermal expansion behavior of $FeCoCrNi_2Al$ high entropy alloy. *Adv Powder Technol* 2021; 32(2): 378–384.
77. Zhang Y, Liu M, Sun J, et al. Excellent thermal stability and mechanical properties of bulk nanostructured FeCoNiCu high entropy alloy. *Mater Sci Eng, A* 2022; 835: 142670.
78. RozmanDetrois KAM, LiuGao TMC, JablonskiHawkLiu PDJA, et al. Long-term creep behavior of a CoCrFeNiMn high-entropy alloy. *J Mater Eng Perform* 2020; 29: 5822–5839.
79. Li W, Chen S and Liaw PK. Discovery and design of fatigue-resistant high-entropy alloys. *Scr Mater* 2020; 187: 68–75.
80. Song C, Li G, Li G, et al. Tensile creep behavior and mechanism of CoCrFeMnNi high entropy alloy. *Micron* 2021; 150: 103144.
81. Joseph J, Stanford N, Hodgson P, et al. Understanding the mechanical behaviour and the large strength/ductility differences between FCC and BCC AlxCoCrFeNi high entropy alloys. *J Alloys Compd* 2017; 726: 885–895.
82. Zhang W, Ma Z, Li C, et al. Micro/nano-mechanical behaviors of individual FCC, BCC and FCC/BCC interphase in a high-entropy alloy. *J Mater Sci Technol* 2022; 114: 102–110.
83. Shivam V, Basu J, Shadangi Y, et al. Mechano-chemical synthesis, thermal stability and phase evolution in AlCoCrFeNiMn high entropy alloy. *J Alloys Compd* 2018; 757: 87–97.
84. Sivaprasad K, Muthupandi V and Szpunar JA. Characterization of nanocrystalline AlCoCrCuNiFeZn high entropy alloy produced by mechanical alloying. *Procedia Materials Science* 2014; 5: 1020–1026.
85. Ji W, Wang W, Wang H, et al. Alloying behavior and novel properties of CoCrFeNiMn high-entropy alloy fabricated by mechanical alloying and spark plasma sintering. *Intermetallics* 2015; 56: 24–27.
86. Wang W-R, Wang W-L and Yeh J-W. Phases, microstructure and mechanical properties of alxcocrfeni high-entropy alloys at elevated temperatures. *J Alloys Compd* 2014; 589: 143–152.
87. Zhang C, Zhang F, Diao H, et al. Understanding phase stability of al-co-cr-fe-ni high entropy alloys. *Mater Des* 2016; 109: 425–433.
88. Luo K, Liu S, Xiong H, et al. Mechanical properties and strengthening mechanism of aluminum matrix composites reinforced by high-entropy alloy particles. *Met Mater Int* 2022; 28: 2811–2821.
89. Pandey V, Seetharam R, Chelladurai H, et al. Fabrication and characterization of Al alloy composites reinforced with nanocrystalline $Al_4CrFeMnTi_{0.25}$ high-entropy alloy particles via double ultrasonic stir casting for aerospace applications, *J Alloys Compd*, 1010, 2025, 177900.
90. An X, Li F, Kan L, et al. High entropy alloy particle reinforced 6061 aluminum matrix composites: an investigation of mechanical strength and thermoelectric properties. *J Alloys Compd* 2025; 1010: 177424.
91. Liu G, Dang T, Hu N, et al. Effect of deep cryogenic treatment on microstructure and mechanical properties of $Fe_{50}Mn_{30}Co_{10}Cr_{10}$ high entropy alloy fabricated by laser metal deposition. *J Alloys Compd* 2024; 1005: 176190.
92. Dwivedi SP, Sharma S, Li C, et al. Exploring microstructural, interfacial, mechanical, and wear properties of Al-$Si_7Mg_{0.3}$ composites with TiMOVWCr high-entropy alloy powder. *ACS Omega* 2024; 9(17): 18813–18826.
93. Huang X, Zhang J, Miao J, et al. On the interactions between molten aluminum and high entropy alloy particles during aluminum matrix composite processing. *J Alloys Compd* 2022; 895(Part 2): 162712.
94. Zhu D, Chen T, Jin X, et al. Quasi-static and dynamic deformation of aluminum matrix composites reinforced by core-shell Al35Ti15Cu10Mn20Cr20 high-entropy alloy particulates. *J Mater Res Technol* 2024; 30: 1009–1019.
95. Lyu P, Chen Y, Liu Z, et al. Surface modification of CrFeCoNiMo high entropy alloy induced by high-current pulsed electron beam. *Appl Surf Sci* 2020; 504: 144453.
96. Cai J, Zu Z, Li C, et al. Hot corrosion behavior of arc ion plating NiCoCrAlYSiHf coating via high-current pulsed electron beam. *Oxid Met* 2020; 94: 569–586.

97. Toroghinejad MR, Taali S, Asgari H, et al. The role of strain path changes on the microstructure, texture, and mechanical properties of unidirectionally and cross-accumulative roll-bonded (ARBed) aluminum. *J Mater Res Technol* 2023; 26: 2165–2178.
98. An X, Li F, Kan L, et al. Synergistic enhancement of 7075 aluminum alloy composites via high entropy alloy particle integration: microstructural and mechanical insights. *Mater Chem Phys* 2024; 328: 129988.
99. Jamaati R, Naseri M and Toroghinejad MR. Wear behavior of nanostructured Al/Al_2O_3 composite fabricated via accumulative roll bonding (ARB) process. *Mater Des* 2014; 59: 540–549.
100. Heydari V, Alizadeh M and Pashangeh S. Investigation into microstructural and mechanical properties of Al–Sn alloy fabricated using accumulative roll bonding combined with heat treatment. *J Mater Res Technol* 2023; 26: 3481–3495.
101. Zhang X, Li R, Huang L, et al. Influence of in-situ and ex-situ precipitations on microstructure and mechanical properties of additive manufacturing CoCrFeMnNi high-entropy alloys. *Vacuum* 2021; 187: 110111.